Integrated Electro-Optic Modulators: Progress, Challenges, and Opportunities

Matthew Yeh
John A. Paulson School of Engineering and Applied Sciences, Harvard University, Cambridge, MA 01238

(Dated: December 13, 2020)

Electro-optic modulators are essential components in modern communication systems and are additionally expected to play an important role in future quantum networks. While bulk modulators are a well-established technology, their large size introduces additional loss that drives up power consumption. Integrating modulators at the chip-scale has therefore been an active area of research. We review the current state of the art in relation to key figures of merit such as bandwidth, loss, and energy consumption. As a specific case, we consider how 2D materials may be used to overcome the performance limits of silicon photonics, and conclude that this is a promising direction, although wafer-scale integration and device optimization are open challenges.

I. INTRODUCTION

Modulation of light forms the backbone of many modern applications. Most prominently, it is a key step in fiber optic communication systems, converting electronic signals into modulated light that can be transmitted over long distances with low loss. On shorter length scales, optical interconnects have also gained much interest as potential replacements for traditional metal interconnects, which suffer from issues such as resistive loss, crosstalk, and limited bandwidth [1]. Because optical signals operate at high carrier frequencies and can be guided in dielectric waveguides instead of metal, photonic systems can offer an intrinsic advantage. In fact, for over a decade the International Roadmap for Devices and Systems (IRDS) has listed optical interconnects as a possible solution for increasing data rates and reducing energy consumption [2].

In this review, we focus on electro-optic modulators (EOMs) that can be integrated at the chip scale. Tremendous research effort has been undertaken to develop devices that can achieve high bandwidths, low operating voltages, small footprints, and CMOS compatibility. In relation to these figures of merit, we present the current state of the art, involving well-studied photonic platforms such as silicon, lithium niobate, and III-V semiconductors. In recent years, research interest in using 2D materials such as graphene and transition metal dichalcogenides (TMDCs) for practical applications has greatly expanded. Thus we will also discuss how this new class of materials may be used to further push the performance limits of integrated EOMs, and in particular consider recent demonstrations of high-performance composite photonic platforms. We conclude that this direction is promising, although much work remains in terms of scalability and device optimization, as well as understanding the fundamental operating mechanisms.

II. PRELIMINARIES

A. Electro-Optic Effect

Many distinct physical mechanisms can lead to an "electro-optic" effect. These can roughly be classified as either electro-refractive or electro-absorptive, where an applied electric field alters the index (n) or the absorption (α), respectively. For the purposes of this paper, we restrict our discussion to devices based on refractive index modulation. It is well-established in optical fiber communications that electroabsorption modulators are high-quality intensity modulators with bandwidths in the 10s of GHz, low operating voltages, and small chirp [3]. However, future applications such as photonic quantum computing and optical neural networks require additional functionality such as phase shifters [4]. Moreover, phase modulation is necessary to employ complex digital modulation schemes such as quadrature amplitude modulation (QAM) that increase communication rates by encoding several bits per symbol [5]. Since electro-refractive effects change the optical path length, phase functionality arises naturally and it is thus of great interest to develop integrated EOMs based on such mechanisms.

Pockels and Kerr Effect: For slow-varying applied electric fields E (compared to optical frequencies), the refractive index in isotropic media can be Taylor-expanded as:

$$n(E) \approx n_0 - \frac{1}{2} r n_0^3 E - \frac{1}{2} s n_0^3 E^2 + \cdots$$

The second term incorporates the Pockels, or linear electro-optic effect, with r the Pockels coefficient. The Pockels effect only is significant in non-inversion symmetric media. If a material had inversion symmetry, then the electro-optic effect should be invariant upon switching the direction of the applied electric field, which means all odd order terms need to vanish. In contrast, the third term incorporates the Kerr, or quadratic electro-optic effect, with k the Kerr coefficient.

The Kerr effect occurs in all materials, although it is much weaker than the Pockels effect so in practice most electro-refractive modulators use the Pockels effect. Importantly, these effects are appealing for high-frequency operation since the refractive index changes occur on femtosecond timescales [6]. It is worth nothing that in anisotropic media the analysis becomes more involved: the Pockels coefficient becomes a rank-3 tensor r_{ijk} and the Kerr coefficient a rank-4 tensor s_{ijkl}. However, symmetry conditions can usually be used to reduce r to a 6×3 matrix and s to a 6×6 matrix.

Free Carrier Plasma Dispersion: Applying a voltage bias changes the carrier concentration in a semiconductor, which will therefore change the absorption (free-carrier absorption) [7]. From the Kramers-Kronig relations, it is known that dispersion and absorption are intimately related and thus a change in refractive index can accompany a change in the absorption spectrum. Experimentally, this effect may be achieved using carrier accumulation in a MOS capacitor structure, carrier injection using a forward biased p-i-n diode, or carrier depletion using a reverse-biased p-n junction.

Franz-Keldysh and Quantum-Confined Stark Effect: The Franz-Keldysh Effect (FKE) can be understood as a tunneling effect. Applying an electric field causes band-bending in a semiconductor, enabling electron and hole wavefunctions to slightly tunnel into the forbidden gap. This results in a redshift of the absorption edge. The Quantum-Confined Stark Effect (QCSE) can be viewed as an extension of the FKE to quantum well structures. In addition to reduced interband energy difference due to band-bending, because the electron and hole are confined within the well region, energy level broadening is reduced and QCSE results in sharper absorption edges than in bulk material. While these effects are normally considered when designing electro-absorption modulators [3], from the Kramers-Kronig relations both FKE and QCSE will give rise to electrorefraction, which finds usage in certain phase modulator implementations.

B. Figures of Merit

Standard figures of merit for modulators include modulation bandwidth/speed, insertion loss, footprint, and energy consumption [8].

Modulation Bandwidth/Speed: Typically defined as the frequency when the modulation drops to half (-3 dB) of its maximum value.

Insertion Loss: Defined as the optical power lost when the modulator is inserted into the photonic circuit. Loss is generally size-dependent, so it is often useful to consider loss per unit length, or loss in a device length L_π required to induce a π phase shift (for phase modulators).

Footprint: This figure of merit is application-dependent, e.g. for interconnects a small footprint is desired, but such devices typically have narrow-band operation. On the other hand, larger devices tend to use more energy because of larger propagation losses.

Energy consumption: Typically defined as the energy consumed per bit. It is thus an important figure of merit for optical interconnects to be suitable replacements for traditional electronic interconnects, with some estimates targeting modulator energies <10 fJ/bit.

Another common figure of merit is known as the half-wave voltage (V_π). However, it is not standard to all modulators as it specifically refers to devices based on Mach-Zehnder interferometers (MZI). In these devices, a Y-junction equally splits the input light between two arms. Applied voltage induces a phase shift in either one or both (push-pull configuration) arms, resulting to interference when recombined at the output Y-junction (Fig. 1A). V_π is then defined as the voltage required to induce a π phase shift between the arms. A related figure of merit is the modulation efficiency $V_\pi L$ (units V·cm), which to some degree incorporates the EOM footprint.

For resonant structures, the figure of merit is the tuning efficiency (units pm/V). These devices typically operate by having a transmission highly sensitive to changes in refractive index. Thus, electrically-induced index changes can be used to switch the resonator on and off resonance, thereby modulating a probe beam (Fig. 1B).

III. STATE OF THE ART

A. Lithium Niobate

Lithium niobate (LN) is well-suited for high-performance EOMs due to its high transparency and and large Pockels coefficient (30 pm/V). Consequently, bulk LN modulators are a widespread technology, although they generally require large $V_\pi L$'s and centimeter-scale lengths. This is attributed to the difficulty of patterning high-index contrast LN waveguides, resulting in weakly confined optical modes that hinder efficient electro-optics since electrodes have to be placed far from the waveguide to avoid propagation loss [9, 10].

In recent years, much progress has been made to develop high-quality thin-film LN on insulator (LNOI) wafers and dry-etching techniques that do not introduce additional losses. Waveguides with silica cladding (index contrast $\Delta n = 0.67$) can be readily fabricated, compared to conventional ion-diffused cladding ($\Delta n = 0.02$) [11, 12]. The enhanced mode confinement enables more efficient electrode placement, resulting in state-of-the-art $V_\pi L$'s of of 1.8-2.8 V·cm, 45-100 GHz bandwidths, <0.5 dB insertion loss, and data transmission rates up to 210 Gbps in the original demonstrations with MZI modulators (Fig. 1A). More recently, a data rate up to 320

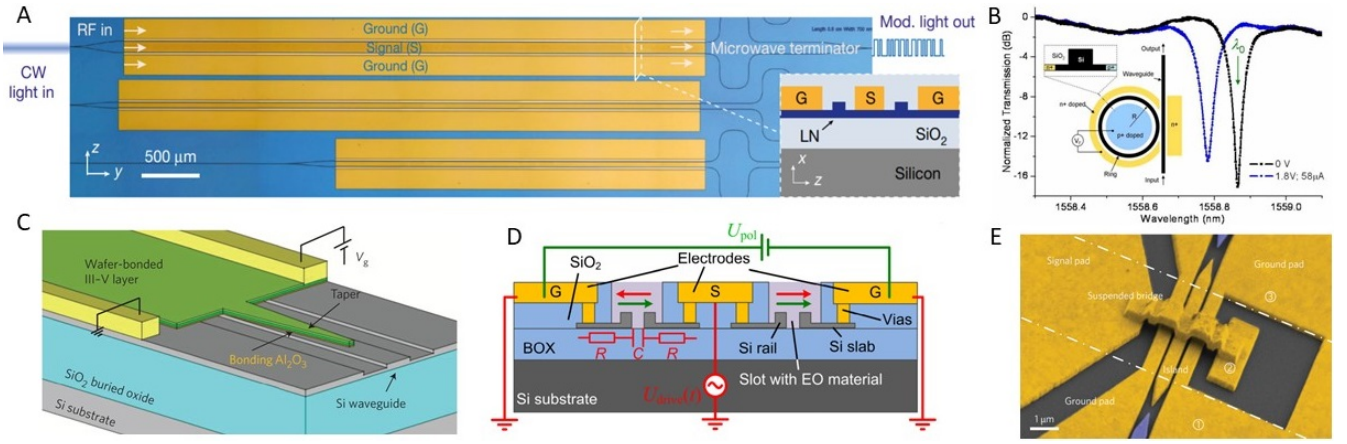

FIG. 1. Operating Mechanism of Selected EOMs. A) Operation principle of LN MZI traveling wave modulators [12]. B) Operation of Si ring modulator. Injected carriers change the resonance condition [18]. C) Hybrid III-V/Si modulator schematic. Applied voltage causes carrier accumulation in the MOS capacitor, changing the index [25]. D) Hybrid polymer/Si modulator schematic, showing polymer deposition within Si slot waveguides [30]. E) False-colored plasmonic MZI modulator SEM image [31].

Gbps was demonstrated using 16-QAM (4 bits encoded per symbol, i.e. each unique in-phase/quadrature pair), although at the cost of higher energy per bit [13].

The primary drawback of the MZI configuration is the large footprint (millimeter lengths). To this end, resonant structures such as microrings and photonic crystal nanobeam cavities have been demonstrated to reduce the footprint to as low as 30 µm length for nanobeams [11, 14]. Notably, the small mode volume of the nanobeam enables a greater tuning efficiency (16 pm/V) than microrings (7 pm/V), although the electrodes have yet to be optimized to achieve a low RC time constant and corresponding high bandwidth. It should be noted that resonant modulation is inherently narrowband and sensitive to fabrication inhomogeneities, limiting applicability.

B. Silicon

The primary benefit of silicon is its compatibility with semiconductor foundries, given that the entire microelectronics industry is built around it. However, as an electro-optic material silicon does not have a strong Pockels/Kerr effect nor a strong Franz-Keldysh effect, particularly at relevant telecom bands at 1.3 µm and 1.5 µm [8]. Thus, index modulation has to be achieved using free carrier plasma dispersion, which inherently occurs on slower time scales than the Pockels effect. Experimentally, the index change at 1550 nm was extracted to be

$$\Delta n = -[8.8 \times 10^{-22}(\Delta N_e) + 8.5 \times 10^{-18}(\Delta N_h)^{0.8}]$$

where ΔN_e, ΔN_h are the injected electron and hole concentrations, respectively (units cm^{-3}). However, this accompanies a corresponding absorption change, so silicon EOMs generally feature larger insertion losses.

$$\Delta\alpha = 8.5 \times 10^{-18}(\Delta N_e) + 6.0 \times 10^{-18}(\Delta N_h)$$

Heroic effort has been dedicated to developing silicon EOMs at the limits of what is achievable with carrier dispersion. The first demonstration of >1 GHz bandwidth employed carrier accumulation in a MOS capacitor [15]. Since accumulation only involves majority carriers, modulation efficiency can be quite high ($V_\pi L \sim 0.2$ V·cm) [16]. Additionally, modulation speed is limited mostly by the RC time constant instead of slow carrier generation or carrier recombination processes. This is the main issue in injection schemes using a p-i-n diode, although microring resonator schemes can get around this somewhat, achieving data rates >12.5 Gbps with diameters as low as 16 µm (Fig. 1B) [17, 18]. Still, the RC time constant in accumulation schemes can be quite limiting, and many of the fastest silicon EOMs are based on carrier depletion effects, where modulating a reverse bias on a p-n junction manipulates the depletion width and thereby the index [20-22]. The speed stems from the fact that sweeping out carriers via drift can occur on picosecond timescales, although at the cost of efficiency. Indeed, such devices have been reported with data rates as high as 100 Gbps [20].

C. III-V Semiconductors

III-V compound semiconductors are widely used in high performance photonic devices. For example, they offer the capability to directly integrate electroabsorption modulators with a distributed feedback laser as the light source [3]. While such a device nominally only offers amplitude modulation, the QCSE can additionally introduce electro-refractive changes and thus phase functionality. This is the basis of most InP-based MZI EOMs, which can offer bandwidths as high as 67 GHz and low $V_\pi L$'s of 0.5-0.6 V·cm [23, 24].

Interestingly, another direction has been to improve standard silicon photonics via heterogeneous integration of III-V semiconductors [25, 26]. Essentially, the idea is the same as accumulation-based schemes, except the electrorefractive layer is now a III-V semiconductor InGaAsP, which possesses larger refractive index changes and smaller absorption changes than silicon (Fig. 1C). Correspondingly, these material properties enable large improvements to loss and modulation efficiency in silicon photonics, with insertion loss <1 dB and $V_\pi L < 0.1$ V·cm. Note that at present these devices have not yet optimized contact resistance, so the bandwidth is currently limited to <2.2 GHz in depletion mode.

D. Polymers

Polymers have a number of properties that make them especially suitable for high-speed and low voltage operation. In particular, they have minimal absorption and can be doped with electro-optic molecules (chromophores) to achieve Pockels coefficients >180 pm/V over a broad range of wavelengths, including telecom bands [27-30]. Initial demonstrations focused on taking full advantage of the polymeric design space, carefully choosing core and cladding materials to eliminate dielectric losses, resulting in ultrahigh bandwidths between 150-200 GHz [27].

More recently, the favorable electro-optics of polymers has been adapted to silicon photonics to create hybrid silicon-organic EOMs [28-30]. These devices generally operate by having a silicon slot waveguide whose core material is injected with the polymer (Fig. 1D). Impressively, these hybrid devices consistently achieve bandwidths >100 GHz and low $V_\pi L$ of <1.1 V·cm, while having sub-millimeter device lengths. However, long-term stability continues to be an active research challenge, with common degradation sources both optical (photobleaching) and thermal (glass transitions, chromophore reorientation) in nature.

E. Plasmonics

Instead of changing the active material, an alternate approach to achieving high-performance EOMs is to convert laser light into surface plasmon polaritons (SPPs). Intuitively, the strong electromagnetic field localization associated with SPPs, which can be below the diffraction limit, makes plasmonics an attractive platform for achieving ultracompact modulators.

These devices generally make use of intuition from traditional MZI and ring resonator implementations. In a plasmonic MZI modulator, input light is converted into SPPs, split along two arms, and sent through a metal-insulator-metal slot waveguide filled with a Pockels material to introduce a phase shift (Fig. 1E) [31, 32]. The SPPs are then interfered, and will only outcouple to a silicon waveguide if in phase. Intriguingly, the index change between the two arms is quite high (~ 0.1), which is attributed in part to stronger confinement and in part to a slower propagation velocity (increased interaction time) than in a photonic waveguide [32]. In conjunction with device area of a few μm^2 and corresponding small RC constant, these characteristics can lead to high bandwidths (>70 GHz) and modulation efficiencies (<0.006 V·cm). However, the electron motion component of an SPP results in ohmic insertion losses up to 10 dB. This can be somewhat mitigated using a plasmonic ring resonator instead of a MZI. The principle of operation is essentially the same as a typical ring modulator, with the key idea being that ohmic loss is intentionally used to attenuate the signal when on resonance. Loss can thereby be reduced to ∼2.5 dB, comparable to silicon EOMs [33].

IV. COMPOSITE PLATFORMS WITH 2D MATERIALS

Since the discovery of graphene, the 2D material designation has greatly expanded to include other systems such as transition metal dichalcogenides (TMDCs). Increasing attention has been paid to the potential of these materials to outperform their bulk counterparts in electronic and photonic applications, such as modulators [34, 35]. For example, they can operate over a wide range of wavelengths and possess strong nonlinear optical response. Moreover, since the layered construction is from weak van der Waals forces instead of covalent/ionic bonding, in principle 2D materials offer easier integration with a variety of materials, since the restriction of lattice matching for epitaxial growth is relaxed. It is thus an ongoing research challenge to develop practical devices that fully take advantage of these properties.

Interestingly, while many EOM prototypes have been demonstrated, especially with graphene, until recently almost all employed electro-absorptive effects [36-38]. In this section, we discuss the current state of the art in 2D-based phase modulation: composite platforms with silicon.

A. Graphene-Silicon

Graphene-based modulators mainly operate using a principle known as Pauli blocking (Fig. 2A). Briefly, by tuning the Fermi level (E_F) via electrostatic doping, interband transitions with energy below $2E_F$ become forbidden [39]. If $E_F > 0$, this arises because the final electron state is occupied (Pauli exclusion); if $E_F < 0$ it is because the initial electron state is empty. Due to the Kramers-Kronig relations, this can also give rise to strong electro-refractive response. While requiring 10s of volts to operate, initial studies of phase modulation importantly demonstrated hybrid graphene-silicon (Gr-Si) waveguides with effective index changes $> 10^{-3}$, compa-

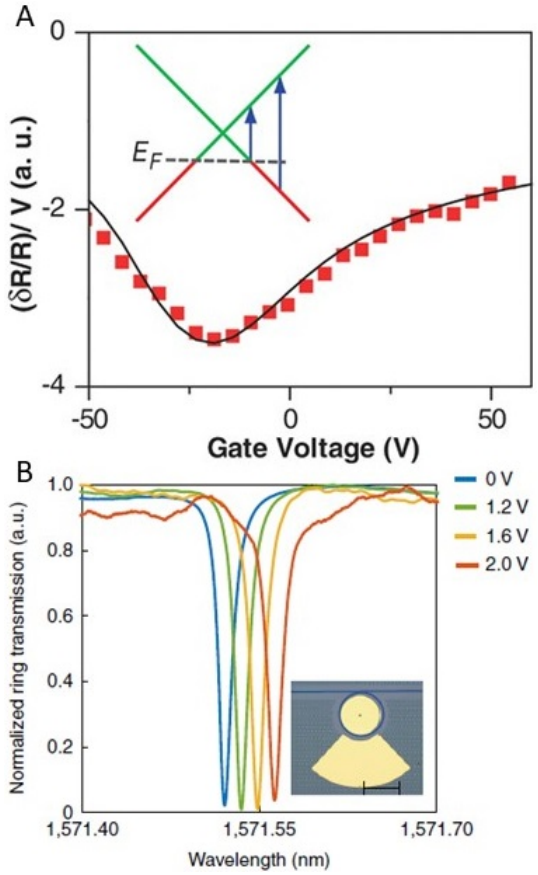

FIG. 2. Electro-Optics with 2D Materials. A) Normalized change of graphene reflectivity reveals how interband transitions vary with gate bias. (Inset) Pauli blocking occurs when $h\omega < 2|E_F|$, where $E = 0$ at the Dirac point [39]. B) Normalized transmission of SiN ring resonator with applied bias to WS_2 monolayer, showing clear redshift with negligible broadening. This indicates minimal change in absorption despite a significant doping-induced index change.(Inset) Optical micrograph of device [45].

rable to or better than what is achievable with free carrier dispersion in silicon photonics [40, 41]. Thus, when operating at transparent wavelengths in the Pauli blocking regime, Gr-Si conceivably offers both large electro-refractive response and small absorption.

A recent demonstration indicated Gr-Si MZI modulators can achieve a impressive modulation efficiency of 0.28 V·cm and 5 GHz bandwidth in a compact footprint ($L \sim 400\,\mu m$) [42]. Importantly, the authors also used the modulator for 10 Gbps data transmission, paving the way for practical usage of 2D-based phase modulators. Unfortunately, the device was operated in a regime where changes in index correlated with increases in absorption, resulting in an impractically large insertion loss $\sim 9\,dB$ (corresponding to 236 dB/cm). This was attributed to poor material quality, specifically low graphene mobility. It is interesting to consider if employing a thin spacer layer of hexagonal boron nitride to create a smooth interface would help enable mobilities $> 10\,000\,cm^2\,V^{-1}\,s^{-1}$ as in the original paper by Geim and Novoselov, although this adds additional fabrication complexity [43, 44].

B. TMDC-Silicon Nitride

Like graphene, the optical properties of TMDCs can also be tuned with electrostatic doping. Studies typically investigate behavior near excitonic resonances, where absorption and thus loss is high. Doping-dependent behavior far from resonances was investigate just recently, in a composite WS_2-silicon nitride (SiN) platform [45]. Intriguingly, at these wavelengths ($\sim 1.55\,\mu m$) the real part of the WS_2 refractive index changes dramatically ($\Delta n = 0.53$) while the imaginary index changes minimally ($\Delta k = 0.004$), a higher ratio than any other platform based on carrier-induced phase shifts. This potential was immediately realized in proof-of-concept MZI phase modulators with low WS_2 insertion loss (0.55 dB) and high modulation efficiency ($V_\pi L = 0.8$ V·cm), albeit with moderate bandwidth (0.3 GHz) and footprint ($L_\pi = 1.2\,mm$).

Still, many of these drawbacks are engineering optimizations and the uniquely large $\Delta n/\Delta k$ merits further investigation. It is worth nothing that the device geometry is not yet optimized to take full advantage of the WS_2 index modulation. In particular, when integrated in a TMDC-HfO_2-ITO capacitor the mode overlap of the SiN waveguide with the monolayer is only 0.03%, resulting in a maximum (but still significant) effective index of change of $\Delta n_{eff} = 1.3 \times 10^{-3}$. Designing structures with better mode overlap could enable even greater modulation efficiencies, which would additionally reduce footprint and thus loss. Alternatively, obtaining a better understanding of the source of the strong electro-refractive response could motivate the design/search of other 2D materials with even better electro-optic properties.

V. DISCUSSION

Table I presents a summary of representative EOMs discussed in this work. Clearly, no platform completely integrates low loss, high bandwidth, and high efficiency while still maintaining compact footprints, although the timeline indicates that much progress has and continues to be made. Ultimately, tradeoffs will have to be made depending on the application. For example, LN modulators appear to be near optimal as long as sub-millimeter size is not critical, so they might find application in quantum photonics (where loss is critical) or high-speed low-power data communications. Alternatively, silicon CMOS compatibility is often cited as a motivation for developing hybrid platforms. To this end, III-V semiconductors and 2D materials are highly appealing due to their large electro-refractive responses and low loss, although at present both need to address

TABLE I. Brief summary of representative EOMs. For resonance-based modulation (denoted by *), tuning efficiency (pm/V) replaces V_π. Footprint refers to waveguide length. - indicates that a figure of merit was not provided/not applicable.

Year	Platform	V_π (V)	$V_\pi L$ (V·cm)	Bandwidth (GHz)	Insertion Loss (dB)	Footprint	Energy per Bit
2018 [11]	MZI	9	1.8	15	0.6	2 mm	1.6 pJ
	LN Microring*	-	7	30	1.5	5 mm	240 fJ
2018 [12]	LN MZI	1.4	2.8	45	0.4	20 mm	0.037-14 fJ
	LN MZI	2.3	2.3	80	0.2	10 mm	-
	LN MZI	4.4	2.2	100	0.1	5 mm	-
2020 [13]	LN MZI	3.1	2.3	67	1.45	7.5 mm	-
	LN MZI	1.9	2.4	48	1.8	13 mm	61-120 fJ
2020 [14]	LN Photonic Crystal*	-	16	17.5	2.2	10 µm	22 fJ
2004 [15]	Si MZI (accumulation)	32	8	1	6.7	2.5 mm	-
2014 [16]	Si MZI (accumulation)	-	0.2	-	2.6	0.4 mm	2-3 pJ
2007 [18]	Si Microring* (injection)	-	<50	-	4	30 µm	-
2012 [19]	Si MZI (injection)	11.6	0.29	0.1	1.2	250 µm	0.9 pJ
2014 [20]	Si MZI (depletion)	10	2.4	-	4.2	2.4 mm	500 pJ
2012 [21]	Si MZI (depletion)	16	2.8	>40	3.2	1 mm	4.2 pJ
2015 [22]	Si MZI (depletion)	4.1	0.74	48	7.6	1.8 mm	7.9-8.8 pJ
2017 [23]	InP MZI	1.5	0.54	67	2	3.6 mm	-
2015 [24]	InP MZI	2	-	40	6.5	-	-
2017 [25]	InGaAsP/Si MZI	3.5	0.09	2.2	1	0.25 mm	-
2017 [26]	InGaAsP/Si MZI	0.86	0.047	0.06	0.23	0.5 mm	-
2002 [27]	Polymer MZI	11.3	22.6	150-200	-	2 cm	-
2014 [28]	Polymer/Si MZI	22	1.1	>100	2.5	0.5 mm	-
2015 [29]	Polymer/Si MZI	0.5	0.05	-	6	1 mm	0.7 fJ
2018 [30]	Polymer/Si MZI	2.2	0.11	-	8.5	0.5 mm	-
2015 [31]	Plasmonic MZI	10	0.006	>70	8	6 µm	-
2017 [32]	Plasmonic MZI	12	0.012	>70	6	10 µm	30-110 fJ
2018 [33]	Plasmonic Microring*	-	-	>110	2.5	6 µm	12 fJ
2015 [40]	Gr/Si MZI	75	30	-	40	0.4 mm	-
2017 [42]	Gr/Si MZI	7.25	0.28	5	9	0.4 mm	1 pJ
2020 [45]	WS_2/SiN MZI	6.5	0.8	0.3	0.55	1.2 mm	-

contact resistance issues so as to increase bandwidth. Although wafer-scale integration is challenging, i.e. III-V materials require wafer bonding or epitaxial growth at CMOS-incompatible temperatures, while 2D material growth and/or large-area transfer methods are still a developing field, much progress has been made in this direction [46-48]. Therefore, the future may see hybrid 2D platforms evolve in parallel with hybrid III-V platforms to fill the silicon photonics opportunity, serving complementary roles as "new" and "old" materials respectively.

It is also interesting to note that EOMs often feature some sort of voltage-bandwidth trade-off, even if the operating mechanisms differ [9, 10]. For example, in MOS structures thinning oxide enables better electrical control (essentially, a larger capacitive voltage divider), reducing V_π [25]. However, this is directly because the capacitance increased, which degrades bandwidth correspondingly. In traveling-wave MZI configurations, where a radiofrequency modulation signal co-propagates with the optical signal, increasing the device length can reduce V_π since there is more length to acquire phase (i.e. $\Delta n(V)$ can be smaller). However, any mismatch in the group velocities will degrade the bandwidth, with stronger effects at longer device lengths [9-10, 12]. As this can be a major limiting factor in device performance, it is thus of interest to determine where these new platforms lie. High voltage-bandwidth performance (30 GHz/V) has already been demonstrated in LN devices [12], so this information could provide a better understanding of how good composite platforms can be in relation to the current state of the art.

VI. CONCLUSION

In conclusion, we have provided an overview of recent progress in the development of integrated electro-optic modulators. Over the years, many platforms have been explored and the performance of integrated EOMs has steadily trended upward, although no single platform can definitively be named the best. Rather, each design brings its own unique set of benefits and tradeoffs, and different modulators will be better suited for different applications. As a specific case, we consider how the strong electro-optic response of 2D materials may be used to enhance silicon photonics, and conclude that they are well-suited to serve as a parallel research thrust to similarly-minded composite III-V/Silicon platforms.

[1] D. A. B. Miller, Proc. IEEE **97(7)**, 1166 (2009).
[2] *International Technology Roadmap for Semiconductors*, Semiconductor Industry Association (2009), http://www.itrs.net.
[3] M. Aoki, et al., IEEE J. Quantum Electron **29(6)**, 2088 (1993).
[4] N. C. Harris, et al., Optica **5(12)**, 1623 (2018).
[5] M. Seimetz, *High-Order Modulation for Optical Fiber Transission* (Springer-Verlag, 2009).
[6] R. W. Boyd, *Nonlinear Optics* (Academic Press, 2020).
[7] R. Soref and B. Bennet, IEEE J. Quantum Electron **23**, 123 (1987).
[8] G. T. Reed, et al., Nat. Photonics **4(8)**, 518 (2010).
[9] E. L. Wooten, et al., IEEE J. Sel. Quantum Electron **6(1)**, 69 (2000).
[10] Y. Qi and Y. Li, Nanophotonics , Ahead of print (2020).
[11] C. Wang, et al., Opt. Express **26(2)**, 1547 (2018).
[12] C. Wang, et al., Nature **562(7725)**, 101 (2018).
[13] M. Xu, et al., Nat. Commun. **11(1)**, 1 (2020).
[14] M. Li, et al., Nat. Commun. **11(1)**, 1 (2020).
[15] A. Liu, et al., Nature **427(6975)**, 615 (2004).
[16] M. Webster, et al., 11th International Conference on Group IV Photonics (GFP) (2014).
[17] Q. Xu, B. Schmidt, S. Pradhan, and M. Lipson, Nature **435**, 325 (2005).
[18] Q. Xu, et al., Opt. Express **15(2)**, 430 (2007).
[19] S. Akiyama, et al., Opt. Express **20(3)**, 2911 (2012).
[20] P. Dong, et al., IEEE J. Sel. Top. Quantum Electron **20**, 150 (2014).
[21] D. J. Thomson, et al., IEEE Photonics Technol. Lett. **24**, 234 (2012).
[22] S. S. Azadeh, et al., Opt. Express **23**, 23526 (2015).
[23] Y. Ogiso, et al., J. Light. Technol. **35(8)**, 1450 (2016).
[24] E. Rouvalis, 2015 IEEE Compound Semiconductor Integrated Circuit Symposium (2015).
[25] J.-H. Han, et al., Nat. Photonics **11(8)**, 486 (2017).
[26] T. Hiraki, et al., Nat. Photonics **11(8)**, 482 (2017).
[27] M. Lee, et al., Science **298(5597)**, 1401 (2002).
[28] L. Alloatti, et al., Light Sci. Appl. **3(5)**, e173 (2014).
[29] S. Koeber, et al., Light Sci. Appl. **4(2)**, e255 (2015).
[30] S. Wolf, et al., Opt. Express **26(1)**, 220 (2018).
[31] C. Haffner, et al., Nat. Photonics **9(8)**, 525 (2015).
[32] M. Ayata, et al., Science **358(6363)**, 630 (2017).
[33] C. Haffner, et al., Nature **556(7702)**, 483 (2018).
[34] Z. Sun, A. Martinez, and F. Wang, Nat. Photonics **10(4)**, 227 (2016).
[35] S. Yu, et al., Adv. Mater. **29(14)**, 1606128 (2017).
[36] M. Liu, et al., Nature **474(7349)**, 64 (2011).
[37] M. Liu, X. Yin, and X. Zhang, Nano Lett. **12(3)**, 1482 (2012).
[38] C. T. Phare, et al., Nat. Photonics **9(8)**, 511 (2015).
[39] F. Wang, et al., Science **320(5873)**, 206 (2008).
[40] M. Mohsin, et al., Sci. Rep. **5(1)**, 1 (2015).
[41] V. Sorianello, et al., Opt. Express **24(26)**, 29984 (2016).
[42] V. Sorianello, et al., Nat. Photonics **12(1)**, 40 (2017).
[43] K. S. Novoselov, et al., Science **306(5696)**, 666 (2004).
[44] L. Banszerus, et al., Sci. Adv. **1(6)**, e1500222 (2015).
[45] I. Datta, et al., Nat. Photonics **14(4)**, 256 (2020).
[46] S.-H. Bae, et al., Nat. Mater. **18(6)**, 550 (2019).
[47] K. Kang, et al., Nature **520**, 656 (2015).
[48] J. Cho, et al., Adv. Funct. Mater. **30(6)**, 1907941 (2020).